Ab initio study of the intermolecular potential of Ar–H_2O

G. Chałasiński
Department of Chemistry and Biochemistry, Southern Illinois University, Carbondale, Illinois 62901, and Department of Chemistry, University of Warsaw, ul.Pasteura 1, 02-093 Warszawa, Poland

M. M. Szczęśniak and S. Scheiner
Department of Chemistry and Biochemistry, Southern Illinois University, Carbondale, Illinois 62901

(Received 22 August 1990; accepted 5 November 1990)

The combination of supermolecular Møller–Plesset treatment with the perturbation theory of intermolecular forces is applied in the analysis of the potential-energy surface of Ar–H_2O. The surface is very isotropic with the lowest barrier for rotation of ~ 35 cm^{-1} above the absolute minimum. The lower bound for D_e is found to be 108 cm^{-1} and the complex reveals a very floppy structure, with Ar moving freely from the H-bridged structure to the coplanar and almost perpendicular arrangement of the C_2–water axis and the Ar–O axis, "T-shaped" structure. This motion is almost isoenergetic (energy change of less than 2 cm^{-1}). The H-bridged structure is favored by the attractive induction and dispersion anisotropies; the T-shaped structure is favored by repulsive exchange anisotropy. The nonadditive effect in the Ar_2–H_2O cluster was also calculated. Implications of our results on the present models of hydrophobic interactions are also discussed.

I. INTRODUCTION

The van der Waals complexes of molecular species bound to rare-gas (Rg) atoms are of fundamental importance to our understanding of weak chemical interactions. These complexes are of particular interest since the rare-gas atom may be regarded as a structureless probe of the molecule's shape.

Unfortunately, when one of the interacting species is a polyatomic, spectroscopic determination of structure and energetics, and eventually of the complete potential-energy hypersurface, presents a very complex problem (cf. Maitland *et al*[1]). First, the presence of internal degrees of freedom means that the observed rotation–vibration spectra are considerably more complicated than for the inert-gas dimers. Second, the intermolecular potential is anisotropic. Third, no formal inversion procedure exists at present by which this potential may be determined from spectroscopic data.

Consequently, with few exceptions such as Rg–H_2 (Refs. 2 and 3) and Ar–HCl (Refs. 4 and 5) systems, our current experimental knowledge of intermolecular potentials is limited to isotropic functions extracted from classical experiments and molecular-beam scattering studies, and to inferences based on rotational spectroscopy of the ground vibrational states of molecular clusters.

In such circumstances *ab initio* calculations of rare-gas–polyatomic complexes may be a unique source of direct information on potential-energy surfaces. In this context the *ab initio* approach, which combines perturbation theory of intermolecular forces,[6–8] with the supermolecular Møller–Plesset perturbation theory (MPPT) treatment, has been recently advocated.[9–13] This approach provides, in a consistent way, both the total interaction energy and its well-defined contributions such as electrostatic, exchange, induction, dispersion, and their respective intrasystem correlation corrections.

Such an approach proved to be reliable and efficient in the case of the dimers and trimers of HF, HCl,[11] and Ar,[10] as well as in the study of Ar–NH_3.[12] In particular, the Ar–NH_3 calculations provided estimates of the equilibrium structure and energy in good agreement with the experimental data. A peculiar structure of this complex was resolved on the basis of analysis of the anisotropies of the interaction energy components. The success with Ar–NH_3 prompted us to address a more difficult problem: the intermolecular potential of the Ar–H_2O system. Complexes of rare gases and water are of great interest as prototypical models for hydrophobic interactions.[14,15]

Unfortunately, Ar–H_2O has proven to be difficult to observe spectroscopically, which was attributed to its remarkably isotropic intermolecular potential.[16] For a long time, the only detailed experimental studies of the Ar–H_2O dimer have been the molecular-beam scattering measurements of Bicks *et al.*,[17] and Brooks, Kalos, and Grosser,[18] from which isotropic 12-6-type potential-energy surfaces were extracted, indicating a binding energy of 125 cm^{-1} and an equilibrium distance of 2.9 Å. Very indirect and rough estimates of $D_e = 133$ cm^{-1} and $R_e = 3.4$ Å for the isotropic Lennard–Jones potential came from computer simulations of the solubilities of rare gases in water.[15] Recently, Cohen *et al.* reported high-resolution far-infrared spectra of Ar–H_2O (Ref. 19) and set forth an interpretation in terms of slightly hindered-rotor model[20] (cf. also Hutson[21]). However, they found it difficult to propose an unambiguous equilibrium structure. They concluded that the large-amplitude motions occurring within this complex make it difficult to establish its structure. On the one hand, they expect the complex to be H bonded, as Ar has been shown to act as Lewis acid in a number of complexes including Ar–HF,[22] Ar–HCl,[23] and Ar–CO_2.[24] On the other, if the Ar–H_2O has a structure compatible with Ar–H_2S,[25] then the H_2O symmetry axis is almost perpendicular to the Ar–S axis with a

planar or a nearly planar arrangement of the H_2O and Ar.

The existing *ab initio* calculations[26,27] cannot be considered conclusive either. In particular, Kołos, Corongiu, and Clementi[27] used a simple "SCF + dispersion" model with dispersion energy obtained from bond polarizabilities. Their final potential had an absolute minimum for a planar C_{2v} structure with Ar bound to the hydrogen end of H_2O, 3.75 Å from the oxygen. However, their equilibrium geometry is by no means definitive as their model failed for another Ar-molecule complex: Ar–HCl, where they did not detect Ar–ClH.

It is then not surprising that several experimental groups are currently studying the Ar–H_2O complex. Hutson[21] set forth a model for the vibrational states of an atom-asymmetric top van der Waals complex and used it to interpret the infrared spectra of Ar–H_2O reported by Cohen *et al.*[20] Lascola and Nesbitt[28] performed measurements of near-infrared spectra, and the microwave spectra were obtained by Lovas.[29] van der Waals streching bands were analyzed by Cohen *et al.*[20] We hope that the *ab initio* calculations reported here will also contribute to future accurate and complete determination of the intermolecular potential of Ar–H_2O.

II. METHOD AND DEFINITIONS

The MPPT interaction energy corrections are derived as the difference between the values for the total energy of the dimer and the sum of the subsystem energies, derived in the basis set of the dimer in every order of perturbation theory,

$$\Delta E^{\mathrm{SCF}} = E_{AB}^{\mathrm{SCF}} - E_A^{\mathrm{SCF}} - E_B^{\mathrm{SCF}}, \tag{1}$$

$$\Delta E^{(n)} = E_{AB}^{(n)} - E_A^{(n)} - E_B^{(n)}, \quad n = 2,3,4, \ldots . \tag{2}$$

The sum of corrections through the nth order will be denoted $\Delta E(n)$; thus, e.g., $\Delta E(3)$ will symbolize the sum of ΔE^{SCF}, $\Delta E^{(2)}$, and $\Delta E^{(3)}$. The interaction energy corrections of intermolecular Møller–Plesset perturbation theory (IMPPT) are denoted $\epsilon^{(ij)}$, where i and j refer to the order of the intermolecular interaction operator and the intramolecular correlation operator, respectively.

A. Partitioning of ΔE^{SCF}

ΔE^{SCF} may be decomposed as follows (cf. Ref. 10):

$$\Delta E^{\mathrm{SCF}} = \Delta E^{\mathrm{HL}} + \Delta E_{\mathrm{def}}^{\mathrm{SCF}}, \tag{3}$$

$$\Delta E^{\mathrm{HL}} = \epsilon_{\mathrm{es}}^{(10)} + \epsilon_{\mathrm{exch}}^{\mathrm{HL}}, \tag{4}$$

where ΔE^{HL} and $\Delta E_{\mathrm{def}}^{\mathrm{SCF}}$ are the Heitler–London (HL) interaction energy and the self-consistent-field (SCF) deformation contribution, respectively. ΔE^{HL} is further decomposed into electrostatic, $\epsilon_{\mathrm{es}}^{(10)}$, and exchange components, $\epsilon_{\mathrm{exch}}^{\mathrm{HL}}$, which describe the electrostatic and exchange energy, respectively, obtained with the unperturbed SCF monomer wave functions. ($\epsilon_{\mathrm{exch}}^{\mathrm{HL}}$ differs from the $\epsilon_{\mathrm{exch}}^{(10)}$ from the IMPPT theory by small "zeroth-order exchange" terms; cf. Ref 10.). The deformation effect $\Delta E_{\mathrm{def}}^{\mathrm{SCF}}$ is due to mutual polarization restrained by the Pauli principle. We will also consider the second-order IMPPT approximations to $\Delta E_{\mathrm{def}}^{\mathrm{SCF}}$: the uncoupled Hartree–Fock (UCHF), $\epsilon_{\mathrm{ind}}^{(20)}$, and the coupled Hartree–Fock (CHF), $\epsilon_{\mathrm{ind}}^{\mathrm{CHF}}$, induction energies.

B. Partitioning of $\Delta E^{(2)}$

$\Delta E^{(2)}$ may be decomposed as follows (cf. Ref. 10):

$$\Delta E^{(2)} = \epsilon_{\mathrm{es},r}^{(12)} + \epsilon_{\mathrm{disp}}^{(20)} + \cdots, \tag{5}$$

where $\cdots$ denotes second-order deformation correlation + second-order exchange correlation, $\epsilon_{\mathrm{es},r}^{(12)}$ denotes the second-order electrostatic-correlation energy (caused by the intramonomer correlation effect) in the "relaxed orbital" form,[13] and $\epsilon_{\mathrm{disp}}^{(20)}$ is the so-called "uncoupled Hartree–Fock dispersion energy." The second-order deformation correlation describes the intramonomer correlation correction to the SCF-deformation contribution. It may be interpreted as the induction-correlation energy which allows for exchange effects. The second-order exchange-correlation term is also difficult to decompose rigorously. It encompasses the exchange-correlation effects related to electrostatic-correlation energy and dispersion energy. This total exchange effect can be approximated as follows, provided that the deformation-correlation contribution is negligible:[12,13]

$$\Delta E_{\mathrm{exch}}^{(2)} = \Delta E^{(2)} - \epsilon_{\mathrm{disp}}^{(20)} - \epsilon_{\mathrm{es},r}^{(12)}. \tag{6}$$

C. Other interaction energy terms

Similar to the above, analyses of $\Delta E^{(3)}$ and $\Delta E^{(4)}$ are possible[10] although more complicated. For the dispersion-bound complexes, the $\Delta E^{(3)}$ term is dominated by its dispersion component, $\epsilon_{\mathrm{disp}}^{(21)}$. The other dispersion term, which belongs to $\Delta E^{(3)}$, is the third-order dispersion energy, $\epsilon_{\mathrm{disp}}^{(30)}$. Two-body $\epsilon_{\mathrm{disp}}^{(30)}$ is of secondary importance compared with $\epsilon_{\mathrm{disp}}^{(21)}$, since the former is of third order and the latter of second order with respect to the interaction potential. However, if we are interested in three-body contributions to the interaction energy, then all second-order dispersion terms vanish exactly and $\epsilon_{\mathrm{disp}}^{(30)}$ provides the leading dispersion nonadditivity. It also dominates the $\Delta E^{(3)}$ nonadditivity for dispersion-bound complexes. These remarks are important in the context of calculations for the Ar_2–H_2O system.

D. Calculation of interaction energies

Calculations of all the supermolecular and perturbational interaction terms are performed using the basis set of the whole dimer [dimer-centered basis set (DCBS)]. With supermolecular interaction energies, this prescription amounts to applying the counterpoise procedure of Boys and Bernardi.[30] There is strong evidence that this is the only consistent means of evaluation of interaction energy at the SCF level[31,33–35] as well as at correlated levels.[32,33–35] With perturbation terms the description of subsystem wave functions in DCBS has important implications. First, some unphysical contributions to ΔE^{SCF} (sometimes referred to as "zeroth-order exchange" terms) disappear.[36] Second, it generally improves the description of the exchange,[36] induction, and dispersion terms.[37] It may, however, deteriorate the electrostatic term. Third, using DCBS consistently is absolutely necessary if individual components of interaction energy are extracted by means of subtraction (e.g., $\Delta E_{\mathrm{def}}^{\mathrm{SCF}}$ or $\Delta E_{\mathrm{exch}}^{(2)}$).

All the calculations were carried out using the GAUSSIAN 86 program[38(a)] and the intermolecular perturbation theory package linked to GAUSSIAN 86.[38(b)]

E. Basis sets

For H_2O we used the "medium-polarized" basis set proposed by Sadlej:[39] (10*s*6*p*4*d*/5*s*4*p*) contracted to [5*s*3*p*2*d*/3*s*3*p*]. For Ar we used the basis set proposed by Chałasiński *et al.*:[40] (14*s*10*p*2*d*) contracted to [7*s*4*p*2*d*]. This basis set is hereafter referred to as the *spd* basis set. Additional calculations at the global minimum were carried out with these basis sets augmented with *f*-symmetry orbitals of the following exponents: 0.18 on O (from Ref. 41) and 0.23 on Ar (from Ref. 40) This basis set is referred to as the *spdf* basis set. Finally, we also augmented the basis of H by adding one *d*-symmetry set of orbitals, with exponent 0.18. This largest basis is referred to as *spdf'*. All additional polarization functions had their exponents optimized for dispersion term.

III. RESULTS

A. Anisotropy of interaction energy

The internal geometry of H_2O was assumed to be undistorted by the interaction: the experimental geometry with $r(OH) = 0.9572$ Å and $\Theta(HOH) = 104.524°$ was the same as in Ref. 42. The scan of the potential-energy surface was carried out for the coplanar and perpendicular motions of the Ar atom around water, visualized in Fig. 1. R ranged from 3.5 to 4.25 Å with an increment of 0.25 Å. Θ varied from 0° to 180° in both the coplanar ($\chi = 0°$) and perpendicular arrangements ($\chi = 90°$), with an increment of 20°.

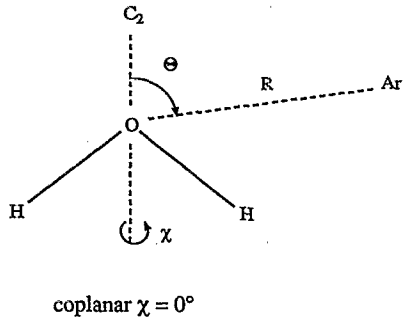

coplanar $\chi = 0°$

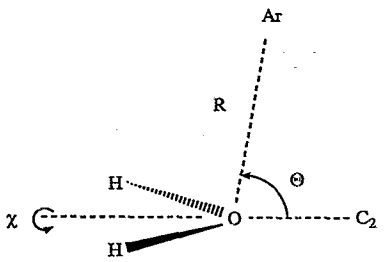

perpendicular $\chi = 90°$

FIG. 1. Definition of the coordinate system for Ar–H_2O. R refers to the O–Ar distance, Θ is the angle between the O–Ar vector and the C_2 axis, χ is the angle between the plane of water and the O–Ar vector.

The values of the total SCF and MP2 interaction energies, ΔE^{SCF} and $\Delta E^{(2)}$, respectively, were obtained with the *spd* basis, at different angles Θ, and at several R, for both the coplanar and perpendicular geometries. They are shown in Table I and Fig. 2. For each value of R the minimum lies in the H_2O plane as seen on the right-hand side of Fig. 2. With respect to the motion of Ar in the H_2O plane, the minimum shifts from 70° for $R = 3.5$ Å to 120° when $R = 4.0$ or 4.25 Å. The minima for these various values of R are very close in energy such that the total potential surface has a very wide and flat region for the coplanar geometry (valley-like), ranging approximately from $\Theta = 70°$ at 3.75 Å to $\Theta = 120°$ at 4.0 Å. At the bottom of this valley the energy differences do not exceed 2 cm^{-1} and it would be extremely difficult to establish the exact position of the absolute minimum. Consequently, the complex of Ar and water should reveal a very floppy structure, from where Ar lies nearly along the O–H bond (hereafter referred to as H-bridged structure), to the almost perpendicular arrangement of the C_2 axis and the Ar–O axis (hereafter referred to as "T-shaped" structure).

Large out-of-plane amplitude is also expected since it would result in only a small increase of the energy. For instance, at $R = 3.75$ Å and $\Theta = 80°$, increasing χ from 0° to 20° results in ~4 cm^{-1} rise of energy. Moreover, moving argon farther around the oxygen in the plane of water, i.e., changing Θ from 80° to 0°, results in the energy change below 10 cm^{-1} when $R = 3.75$ Å. Free motion of Ar around water, in the plane of water at 3.75 Å, is hindered by an energy barrier of less than 35 cm^{-1} with respect to the bottom of the valley. This barrier occurs at $\Theta = 180°$ in the middle of the H–H edge of water.

The anisotropy of the SCF component of the interaction energy is shown in Fig. 3 to be determined principally by the exchange term. The latter term is the most orientation dependent and may be thought of as reflecting the shape of the water molecule. It has a saddle point between the hydrogens, maxima at the hydrogens, and a minimum for "T-shaped" structure. Interestingly, the traditional approximate picture

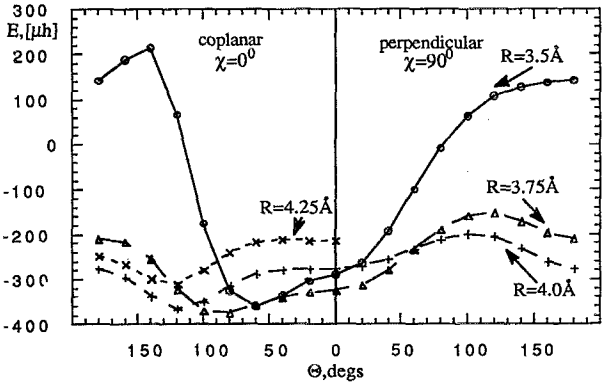

FIG. 2. Θ dependence of the Ar–H_2O interaction energy for different R calculated at the MP2 level of theory.

TABLE I. R and Θ dependence of the ΔE^{SCF} and the total $\Delta E(2)$ interaction energy for Ar–H_2O (for definitions see the text). Energies in μhartrees.

	$R = 3.5$ Å		$R = 3.75$ Å		$R = 4.00$ Å	
	ΔE^{SCF}	$\Delta E(2)$	ΔE^{SCF}	$\Delta E(2)$	ΔE^{SCF}	$\Delta E(2)$
			Coplanar, $\chi = 0°$			
180°	940.96	142.36	346.64	− 209.30	113.06	− 275.84
160°	1064.76	188.39	385.30	− 216.32	122.16	− 294.37
140°	1252.35	214.25	436.78	− 253.81	130.07	− 337.02
120°	1159.67	67.00	393.45	− 321.05	111.74	− 364.90
100°	792.48	− 174.97	267.40	− 369.30	76.23	− 349.90
80°	468.06	− 325.90	156.77	− 373.50	44.73	− 314.01
60°	317.56	− 359.07	101.53	− 356.30	25.08	− 288.02
40°	286.10	− 335.73	84.70	− 339.48	14.27	− 277.90
20°	274.20	− 303.22	83.20	− 328.22	8.60	− 275.90
0°	305.92	− 286.37	83.91	− 324.38	6.7	− 275.97
			Perpendicular, $\chi = 90°$			
20°	327.44	− 262.57	94.54	311.54	12.03	− 269.96
40°	385.02	− 192.06	123.45	− 277.76	26.81	− 254.16
60°	463.54	− 99.76	164.06	− 233.11	48.37	− 232.84
80°	548.70	− 8.60	208.91	− 189.10	72.90	− 211.52
100°	632.96	63.66	250.87	− 158.49	94.73	− 199.06
120°	719.25	108.01	286.23	− 151.80	108.91	− 204.58
140°	813.52	127.94	315.38	− 169.77	114.24	229.69
160°	901.91	137.53	337.60	− 196.81	113.94	− 261.29

of water, having two localized sp^3 lone electron pairs, is not reflected by this shape: moving Ar in the perpendicular plane causes the interaction energy to rise monotonically with no evident irregularity in the hypothetical lone-pair region $\Theta = 50°$, $\chi = 90°$. This conclusion is in contrast to the situation in Ar–NH_3,[12] where the HL-exchange component as well as the SCF interaction energy have a pronounced maximum in the region when the hypothetical lone electron pair of N is directed toward Ar.

The curve which represents the electrostatic component in Fig. 3 (see Table II) looks very much like a mirror image of the exchange curve, albeit flatter. This behavior is attributed to the fact that both terms are overlap dependent. When these terms are added up, their sum (the Heitler–London interaction energy) retains the shape of the exchange term. The SCF-deformation term reveals a somewhat different anisotropy from that of the electrostatic term but is of secondary importance. When the SCF-deformation term is combined with the Heitler–London energy one obtains the entire SCF curve which is thus little changed from the Heitler–London curve, only flatter and displaced to less repulsive energy. However, because of this flatness, in particular in the coplanar geometry, and for $\Theta < 100°$, the absolute minimum of the Heitler–London energy is at 60°, whereas the absolute minimum of the SCF interaction energy is at 0°.

The behaviors of the various post-SCF terms are illustrated in Fig. 4 (see Table II). First, one can see that the anisotropy of the dispersion energy, the major contribution to $\Delta E^{(2)}$, is reciprocal to that of the exchange energy (cf. Fig. 3) and therefore to the SCF interaction energy. Indeed,

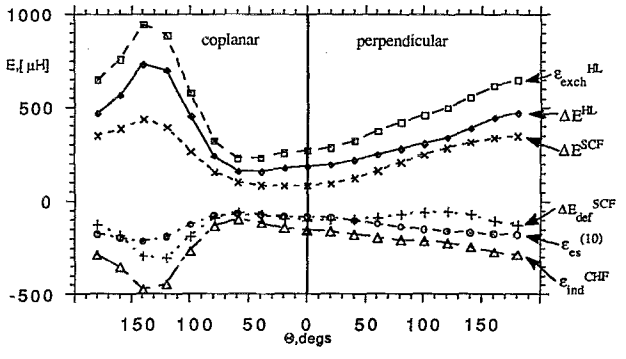

FIG. 3. Θ dependence of the Ar–H_2O interaction energy terms which belong to ΔE^{SCF} (for definitions, see the text). R is kept at 3.75 Å.

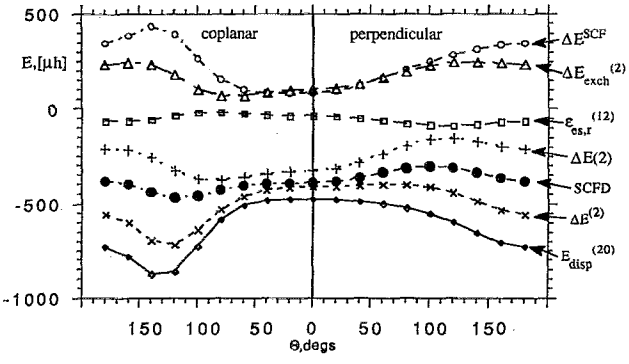

FIG. 4. Θ dependence of the Ar–H_2O interaction energy terms involving correlation (for definitions, see the text). R is kept at 3.75 Å.

TABLE II. Θ dependence of the interaction energy terms for Ar–H_2O at R = 3.75 Å (for definitions, see the text). Energies in μhartrees.

Θ	$\epsilon_{elst}^{(10)}$	ϵ_{exch}^{HL}	ΔE^{HL}	ΔE^{SCF}	$\epsilon_{es,r}^{(12)}$	$\epsilon_{disp}^{(20)}$	$\Delta E^{(2)}$	$\Delta E(2)$	$\Delta E_{exch}^{(2)}$
					Coplanar, $\chi = 0°$				
180°	−177.17	647.35	470.19	346.64	−65.64	−725.98	−555.94	−209.30	235.68
160°	−193.82	760.55	566.72	385.30	−65.39	−780.94	−601.62	−216.32	244.71
140°	−214.70	946.86	732.20	436.78	−57.66	−872.50	−690.59	−253.81	239.57
120°	−188.70	887.98	699.26	393.45	−35.85	−858.71	−714.50	−321.05	180.06
100°	−125.64	579.58	453.93	267.40	−18.27	−723.14	−636.70	−369.30	104.71
80°	−80.62	323.06	242.44	156.77	−17.75	−582.63	−530.27	−373.50	70.11
60°	−69.41	230.16	160.75	101.53	−25.69	−505.12	−457.83	−356.30	72.98
40°	−75.03	232.77	157.74	84.70	−33.00	−478.58	−424.18	−339.48	87.40
20°	−82.46	258.72	176.25	83.20	−37.20	−473.32	−411.42	−328.22	99.10
0°	−85.48	270.99	185.51	83.91	−38.62	−473.04	−408.29	−324.38	103.37
					Perpendicular, $\chi = 90°$				
20°	−90.36	285.50	195.14	94.54	−41.94	−475.61	−406.08	−311.54	111.47
40°	−103.78	323.71	219.93	123.45	−51.26	−484.02	−401.21	−277.76	134.07
60°	−121.49	372.54	251.05	164.06	−64.42	−499.09	−397.17	−233.11	166.34
80°	−138.15	419.02	280.87	208.91	−77.88	−521.16	−398.01	−189.10	201.03
100°	−151.09	459.07	307.98	250.87	−87.50	−551.72	−409.36	−158.49	229.86
120°	−160.44	500.94	340.50	286.23	−89.46	−594.44	−438.03	−151.80	245.87
140°	−167.84	556.54	388.70	315.38	−82.45	−649.89	−485.15	−169.77	247.19
160°	−174.24	618.12	443.88	337.60	−71.22	−703.21	−534.41	−196.81	240.02

J. Chem. Phys., Vol. 94, No. 4, 15 February 1991

the minima in one nearly coincide with the maxima in the other. However, this behavior is not fully reflected in $\Delta E^{(2)}$ because the $\Delta E^{(2)}_{\rm exch}$ term [see Eq. (7)] has the same general shape as $\epsilon^{\rm HL}_{\rm exch}$. It has thus a smoothing effect on the anisotropy of $\epsilon^{(20)}_{\rm disp}$, making its extrema less pronounced and shifting the $\Delta E^{(2)}$ curve higher in energy compared with $\epsilon^{(20)}_{\rm disp}$.

It is also important to note a greater role of $\Delta E^{(2)}_{\rm exch}$ which is as large as the SCF interaction energy for $\Theta \lesssim 100°$ in both the coplanar and perpendicular geometries.

It is worthwhile to comment on the important and popular "SCF + dispersion" (SCFD) approximation.[27,43] The $\Delta E^{\rm SCF} + \epsilon^{(20)}_{\rm disp}$ curve is deeper (since it neglects second-order exchange terms) and flatter than $\Delta E(2)$. It has similar anisotropy, but the quantitative details, such as the position of the minimum, are different. Namely, the minimum occurs at 120° (H-bridged configuration) for $\Delta E^{\rm SCF} + \epsilon^{(20)}_{\rm disp}$ and at 80° for $\Delta E(2)$.

Most of the above conclusions, both at the SCF and correlated levels, are similar to those derived for the Ar–NH_3 complex.[12] However, the total picture is more complicated. The "T-shaped" configuration, and the H-bridged structure at $\Theta = 120°$, lead to interaction energies extremely close to each other and it is difficult to pin down the absolute minimum. Interestingly, the physical origins of these two favorable structures are different. Analysis of the interaction energy decomposition presented in Table III leads to a conclusion that while the former structure minimizes the exchange repulsion effects, the latter structure is favored by the dispersion and SCF-deformation contributions. It should be stressed that all these conclusions are not changed at different levels of theory (SCFD, MP2, MP4) and do not depend on the basis set; cf. Table III.

B. Structure of rare-gas–molecule complexes

Elucidation of structural features of van der Waals complexes based on consideration of the major contributions to the interaction energy is of great importance. The aggregates of polar molecules have been shown to assume the equilibrium geometries determined by the electrostatic interaction.[44,45] The exceptions seem to be well understood and may result from the importance of the exchange (shape) component as well as from more complicated balance of several other components.[45]

When the complex includes at least one nonpolar species the simple electrostatic model is not applicable. A nonpolar system may either have higher permanent multipole moments (quadrupole like N_2 or octupole like CH_4) or not at all (closed-shell atoms, like Ar or Mg). Consequently, the electrostatic interaction (although it is not negligible, even in rare-gas complexes, due to charge penetration effects) cannot be a determining factor.

It has recently been suggested[21,46] that the complexes of rare gases with polar molecules should assume an equilibrium structure determined by the induction interaction. This approach proved to be predictive for the rare-gas–hydrogen halide dimers.[46] However, consideration of only the induction (or the SCF-deformation) component would wrongly predict the H-bridged structure to be the most stable in the Ar–NH_3 case. Such an approach would also underestimate the role of the coplanar, $R = 3.75$ Å, and $\Theta = 80°$ structure of Ar–H_2O. This shortcoming is not surprising since the induction term is quantitatively of secondary importance in the case of rare-gas–molecule interactions. The stability of these complexes results from a balance of the repulsive exchange effects and attractive dispersion forces. Yet, we have to keep in mind that the induction term affects the anisotropy of the total interaction energy and cannot be disregarded. Indeed, if we neglect the SCF-deformation term, the energy of the H-bridged structure will increase substantially more than the energy of "T-shaped" structure, and the qualitative picture of the anisotropy will change.

C. Reliability of potential-energy surface

In order to acquire confidence in our results and conclusions, it is necessary to discuss the accuracy of our calculations.

There are two major sources of errors in *ab initio* calculation of intermolecular forces: (i) unsaturation of the basis set and (ii) approximate treatment of electron correlation effects. Neither is easy to control or estimate. Fortunately, the experience with model systems may be very helpful in this context. Extensive *ab initio* MP4 calculations of the total interaction energy and its components were performed for several dispersion-bound complexes.[33–35,40,47] These studies showed that the electrostatic, exchange, and induction (deformation) energies can be calculated within a few percent of error with extended basis sets, such as those used in this paper. The most demanding term is dispersion, which requires (a) highly correlated treatment of inter-intramonomer electron correlation, beyond the MP2 level, and (b) higher polarization functions, beyond f symmetry. In particular, the lack of higher than f-symmetry polarization functions proved to be a serious shortcoming. It results in underestimated dispersion contribution and too shallow a potential-energy curve.

The results reported in Table III for three basis sets, *spd*, *spdf*, and *spdf'*, and at different levels of theory up through MP4, may be helpful to estimate the error for our results. It turns out that, as in the Ar–NH_3 case, the convergence pattern for supermolecular MPPT in Ar–H_2O resembles very much that of the Ar dimer.[12,40,47] The basis-set dependence of the dispersion term is also similar. Therefore, one may conclude that the accuracy of the Ar_2 calculations and the present calculations should also be similar. Consequently, our results should provide lower bound to the exact values, and the actual error of the *spdf* basis-set results for the total interaction energy may amount to 20%–25% as in Ar_2. This error may be attributed almost entirely to the underestimation of the dispersion term. In Table III one can see that the changes of the basis set affect mostly the dispersion term. All the other terms (except for small electrostatic correlation, $\epsilon^{(12)}_{{\rm es},r}$) are relatively stable and are expected to be accurate within a few percent of their actual value, even with the *spd* basis.

TABLE III. Interaction energy contributions to Ar–H_2O in the coplanar H-bridged, and coplanar and perpendicular arrangement of the C_2 axis and the Ar–O axis. All calculations are full electron calculations unless indicated otherwise. All energies in μhartrees.

	$R = 3.75$ Å, $\Theta = 80°$			$R = 4.0$ Å, $\Theta = 120°$		
Basis	*spd*	*spdf*	*spdf'*	*spd*	*spdf*	*spdf'*
ΔE^{SCF}	156.77	148.05	145.85	111.74	94.14	91.84
$\Delta E^{(2)}$	−528.75[a,b]	−603.75[a]	−616.57	−474.68[a,c]	−543.87[a]	−561.24
$\Delta E^{(3)}$	58.43[a]	56.68[a]		42.97[a]	42.42[a]	
$\Delta E^{(4)}_{DQ}$	27.73[a]	32.05[a]		31.50[a]	21.14[a]	
$\Delta E^{(4)}_{SDQ}$	−0.19[a]	−1.64[a]		2.41[a]	0.68[a]	
$\Delta E^{(4)}$	−71.96[a]	−90.62[a]		−67.10[a]	−84.20[a]	
$\Delta E(4)$	−385.51[a]	−489.64[a]		−387.07[a]	−491.51[a]	
ϵ^{HL}_{exch}	323.07	323.75	323.39	341.08	341.16	340.50
$\epsilon^{(10)}_{es}$	−80.62	−82.98	−83.40	−72.80	−80.62	−79.38
ΔE^{SCF}_{def}	−85.67	−92.72	−94.14	−156.54	−166.40	−169.28
$\epsilon^{(20)}_{ind}$	−114.79	−120.31	−121.43	−176.34	−184.87	−186.58
ϵ^{CHF}_{ind}	−130.99	−137.91	−139.47	−201.37	−211.25	−213.89
$\epsilon^{(12)}_{exch}$	−17.75	−19.46	−17.77	−11.05	−20.30	−17.88
$\epsilon^{(20)}_{disp}$	−582.63	−657.99	−670.23	−542.49	−602.15	−616.96
$\Delta E^{(2)}_{exch}$	71.63	73.70	71.43	76.90	78.56	73.60
$\epsilon^{(21)}_{disp}$	56.72	52.41	50.41	41.48	38.62	35.01
$\Delta E^{SCF} + \epsilon^{(20)}_{disp}$	−425.86	−509.94	−524.38	−430.75	−508.00	−525.12
$\Delta E(2)$	−371.98	−455.70	−470.72	−364.90	−449.70	−470.00

[a] Frozen core result.
[b] Full electron calculations give $-530.27\,\mu$H.
[c] Full electron calculations give $-476.64\,\mu$H.

D. Ar–H_2O complex as a model of hydrophobic effects

The tendency for dissolved nonpolar species to spontaneously adhere to each other in aqueous solutions is thought to be one of the main organizational processes in structural biochemistry and biology, the so-called hydrophobic effect. The origin of this effect may be explained by consideration of the entropic changes of the Gibbs free energy. Yet the details of the hydrophobic associations are far from being understood. Several computer simulations of the water solutions of rare gases[14,15] and methane[48] led to the suggestion that the "solvent-separated" interactions [where two hydrophobic species are separated by a molecule of water, Fig. 5(b)], dominate over the "contact" (neighbor–neighbor) interactions [Fig. 5(a)].[49]

Recently, Ben-Naim[50] questioned this interpretation by pointing out that computer simulations are not accurate enough to enable proposal of a definite structure. In particular, the majority of simulation experiments use an isotropic potential for water–solute interactions. Moreover, the solvent-separated structure [Fig. 5(b)] would block some of the H-bond sites in water. By using a very simple tetrahedral model for a water molecule, Ben-Naim argues that the most likely structure should be the "water-bridged" one [Fig. 5(c)] as it does not block any possible H-bond sites in water.

Our anisotropic Ar–H_2O potential could shed some light on the energetic aspects of this problem. The water-bridged structure may also be inferred from our *ab initio* potential. If an Ar atom has to avoid the H-bond structure it should attack H_2O in the region between the two lone elec-

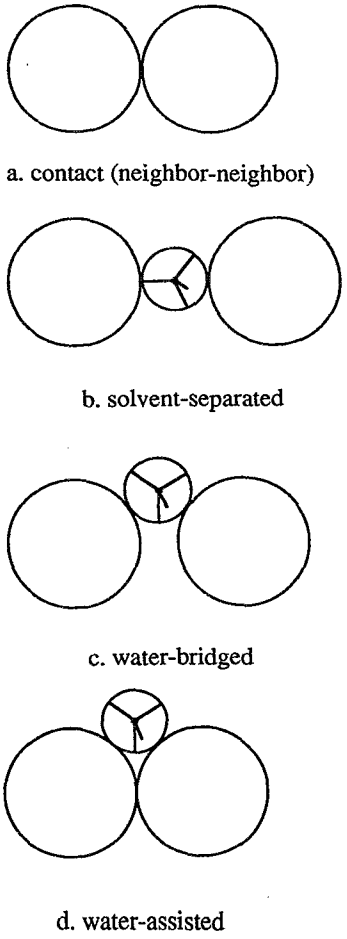

FIG. 5. Possible configurations for two argon atoms and one water molecule which may form in a water solution [cf. Ben-Naim (Ref. 50)]. (a) contact (neighbor–neighbor), (b) solvent separated, (c) water bridged, (d) water assisted.

tron pairs and one O–H bond. A second Ar atom may do the same on the other side of water; [cf. Fig. 5(c)]. These conclusions are in agreement with the model postulated by Ben-Naim. The *ab initio* results provide also other additional interesting details which were not known previously.

First, Ben-Naim's qualitative model of water assumes (1) tetrahedral water, (2) equivalence of lone electron pairs and the O–H bonds, and (3) Ar may approach the water tetrahedron from any face with equal probability. While this may be a reasonable picture for H-bonded complexes it is not for complexes of water with rare gases. In fact, if Ar is to avoid the H-bridged structure, it should approach from the *H–lone-pair–lone-pair* face. The middle of the *lone-pair–lone-pair* edge is only slightly less favorable. On the other hand, the *H–H–lone-pair* faces are definitely worse and the *H–H* edge is the least favorable.

Furthermore, our calculations enable us to assign rough estimates of interaction energies in all the structures shown in Fig. 5 by summing up the two-body interactions (the Ar–Ar potential has been taken from Ref. 40). The solvent-separated structure [Fig. 5(b)] is the least favorable energetically; the interaction energy amounts to roughly $-700\,\mu$H.

The water-bridged structure [Fig. 5(c)] is slightly more favorable. If Ar atoms are situated in the optimal Ar–H_2O positions, i.e., the angle Ar–O–Ar amounts to $2\times 80° = 160°$, the interaction energy amounts to about $-750\,\mu$H. If, as in Ben-Naim's model, Ar atoms are attached to the centers of faces of water tetrahedron the interaction energy is nearly identical. In the structures [Figs. 5(b) and 5(c)] the interaction energy is mainly due to Ar–H_2O interactions, since the Ar atoms are too far apart to allow for any meaningful Ar–Ar contribution. A special case of water-bridged structure in which the Ar–Ar interaction is maximized could be the "water-assisted" structure [Fig. 5(d)] in which two Ar atoms are at their optimal distance (4 Å) and the Ar–O–Ar angle amounts to 64°. This structure is the most stable, $-930\,\mu$H. The nonadditive three-body effect in this structure, which will be discussed below, does not affect this conclusion.

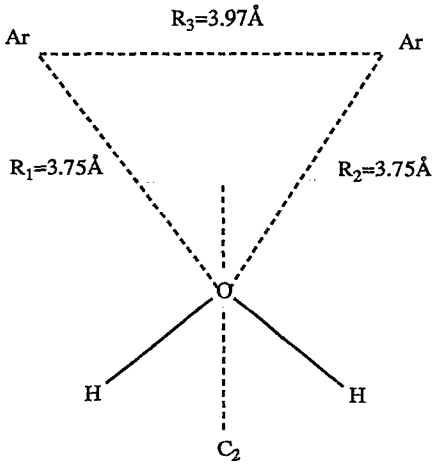

FIG. 6. Configuration of the Ar_2–H_2O complex.

E. Ar_2–H_2O and three-body nonadditivity

In the context of the hydrophobic effect, it is important to analyze the nonadditive effect due to the influence of one water molecule on two Ar atoms. The geometry of the Ar_2–H_2O complex is shown in Fig. 6. This geometry was chosen so as to ensure both the maximal attraction between Ar atoms and almost maximal Ar–H_2O attractions. Therefore, the Ar–Ar distance of 3.97 Å corresponds to R_e in the Ar dimer and the Ar–O distance of 3.75 Å is, according to the results of this paper, optimal for the water–Ar interaction in the water-assisted configuration [Fig. 5(d)].

The values of two- and three-body components are reported in Table IV. One can see that there is a great deal of

TABLE IV. Two- and three-body interaction energy contributions in the Ar_2H_2O complex; geometry in Fig. 6, the *spd* basis. Energies in μhartrees.

	Two body		Three body
	Ar...Ar	Ar...H_2O	
ΔE^{SCF}	193.06	83.32	−8.76
$\Delta E^{(2)}$	−451.14	−418.98	6.22
$\Delta E^{(3)}$	84.46	45.39	9.42
$\Delta E(3)$	−173.62	−290.27	6.88
$\epsilon_{exch}^{(10)}$	285.14	243.16	−14.69
$\epsilon_{es}^{(10)}$	−81.23	−78.09	0[a]
ΔE_{def}^{SCF}	−10.85	−81.75	5.94
$\epsilon_{ind}^{(20)}$	−82.68	−117.32	3.72
$\epsilon_{es,r}^{(12)}$	−20.91	−36.06	0[a]
$\epsilon_{disp}^{(20)}$	−506.78	−476.99	$\epsilon_{disp}^{(30)}$: 9.5
$\Delta E_{exch}^{(2)}$	72.55	94.07	6.22
$\epsilon_{disp}^{(21)}$	87.03	54.13	0[a]

[a] This term is additive.

cancellation among different three-body terms. The total three-body effect of $\Delta E(3)$ is repulsive but does not exceed 2 cm^{-1}. The only attractive contribution arises from exchange effects included in ϵ_{exch}^{HL}. The total SCF nonadditivity is also negative, but the effect of the ϵ_{exch}^{HL} nonadditivity is partly reduced by the nonadditivity of ΔE_{def}^{SCF}. The correlation nonadditivities of $\Delta E^{(2)}$ and $\Delta E^{(3)}$ are repulsive. It is worthwhile to note that the nonadditivity of $\Delta E^{(3)}$ is largely due to the nonadditivity of the third-order dispersion term, $\epsilon_{disp}^{(30)}$.

In conclusion, our results seem to exclude the existence of large many-body effects. However, (1) none of the three-body contributions is negligible, and (2) approximation of the total three-body effect by any of them would be improper. In particular, the approximation of the nonadditive effects by induced-dipole–induced-dipole force as in the recent study of Backx and Goldman[51] is incorrect for two reasons: (a) the induction effect is singled out and (b) the induction effect is a poor approximation to SCF deformation. Consequently, their finding of a significant new repulsive force in the hydrophobic interaction should be questioned.

IV. DISCUSSION AND CONCLUSIONS

To the best of our knowledge, the only recent experimental information on the Ar–H_2O potential comes from two sources: the computer simulations of the solubility of Ar–H_2O by Anderson and collaborators,[14,15] and the far-infrared laser spectroscopy by Saykally and his group.[19,20]

In the computer simulations a Lennard-Jones distance R_e and well depth D_e were established to be 3.44 Å and 133 cm^{-1}, respectively. These estimates must be considered as rather crude, although it may also happen that they are fortuitously fairly good for an isotropic pair potential. It would not be meaningful to guess error bars here.

As to spectroscopic study, Cohen *et al.*[20] determined effective radial potentials for the three lowest Σ-type internal rotor states. The estimates of the well depths for the ground $\Sigma(0_{00})$ and two excited internal rotor states, $\Sigma(1_{01})$ and $\Sigma(1_{10})$, are 126, 153, and 98 cm^{-1}, respectively. On this basis they suggest a well depth of the anisotropic potential of 150 cm^{-1} and the van der Waals distance of 3.6 Å.[20] Again, this must be considered as largely a guess on which it is impossible to place any error bars.

The results presented in this paper are compatible with those discussed above. We showed that the lower bound for D_e is 108 cm^{-1}. The true D_e may be larger by roughly 20%–25%. We also analyzed the anisotropy of the Ar–H_2O potential. On the basis of these results we propose a very floppy coplanar structure of this complex, with Ar moving fairly freely from the H-bridged structure ($\Theta = 120°$ at 4.0 Å) to the almost perpendicular arrangement of the C_2 axis and the Ar–O axis (T-shaped structure, $\Theta = 80°$ at 3.75 Å). This motion is almost isoenergetic (energy change of less than 2 cm^{-1}), and if continued, the Ar atom may move to the other side of water across a barrier of 10 cm^{-1} at $\Theta = 0°$. An arbitrary rotation around water is actually hindered most by the H–H edge of the water tetrahedron and the lowest barrier for this rotation is 35 cm^{-1} above the absolute minimum. Interestingly, the regions where the lone electron pairs of water should be localized according to the sp^3 hybridization model do not lead to any separate barriers on the intermolecular energy surface.

The knowledge of the Ar–H_2O potential surface enables us to shed new light on the character of hydrophobic effects. We found out that the Ar atom can equally well assume the H-bridged structure, as in the hydrophylic interactions, and the coplanar structure, with the Ar atom approaching from the *H–lone-pair–lone-pair* face of water. The latter structure may be characteristic for hydrophobic interactions. Consequently, the hydrophobic arrangement would not differ in energy from the hydrophilic arrangement, and the total hydrophobic effect would reduce to its entropic (organizational) component. It remains to be seen whether this conclusion may be extrapolated to other water complexes involved in hydrophobic phenomena (e.g., complexes with hydrocarbons). Work in this direction is in progress in our laboratory.

Our results provide support for Ben-Naim's suggestion[50] that the "solvent-bridged" complexes should prevail over the "solvent-separated" ones in the solutions of hydrophobic species. Even more, we point out that among the solvent-bridged structures the most favorable may be the "solvent-assisted," i.e., the "contact" argon structures accompanied by a water molecule as in Fig. 5(d). The stability of this structure results from two-body interactions; the three-body term is found very small. In conclusion, it should be pointed out that the T-shaped structure of Ar–H_2O is identical to that in NH_3–Ar (Ref. 12) and PH_3–Ar,[52] which are characterized by the same set of parameters, of $R = 3.75$ Å and $\Theta = 80°$. While the Ar atom can assume a H-bridged position in Ar–H_2O with equal likelihood, this position is strongly disfavored in NH_3–Ar and PH_3–Ar complexes.

ACKNOWLEDGMENTS

This work was supported by the National Institutes of Health (Grant No. GM36912) and by the Polish Academy of Sciences (Grant No. CPBP01.12). We thank the IBM Corporation for the grant of supercomputer time within their Research Support Program.

[1] G. C. Maitland, M. Rigby, E. B. Smith, and W. A. Wakeham, *Intermolecular Forces, Their Origin and Determination* (Clarendon, Oxford, 1981).
[2] A. R. W. McKellar, Faraday Discuss. Chem. Soc. **73**, 89 (1982).
[3] U. Buck, H. Meyer, and R. J. Leroy, J. Chem. Phys. **80**, 5589 (1984).
[4] R. L. Robinson, D. Ray, D. H. Gwo, and R. J. Saykally, J. Chem. Phys. **87**, 5149 (1987); R. L. Robinson, D. H. Gwo, and R. J. Saykally, *ibid.* **86**, 5211 (1987); **87**, 5156 (1987); Mol. Phys. **63**, 1201 (1988).
[5] J. M. Hutson, J. Chem. Phys. **89**, 4550 (1988).
[6] K. Szalewicz and B. Jeziorski, Mol. Phys. **38**, 191 (1979); S. Rybak, K. Szalewicz, B. Jeziorski, and M. Jaszuński, J. Chem. Phys. **86**, 5652 (1987).
[7] B. Jeziorski, R. Moszyński, S. Rybak, and K. Szalewicz, in *Many-Body Methods in Quantum Chemistry*, edited by U. Kaldor (Springer, New York, 1989), p. 65.
[8] K. Szalewicz, S. J. Cole, W. Kolos, and R. J. Bartlett, J. Chem. Phys. **89**, 3662 (1988).
[9] G. Chałasiński and M. M. Szczęśniak, Mol. Phys. **63**, 205 (1988).
[10] G. Chałasiński, M. M. Szczęśniak, and S. M. Cybulski, J. Chem. Phys. **92**, 2481 (1990).
[11] G. Chałasiński, S. M. Cybulski, M. M. Szczęśniak, and S. Scheiner, J.

Chem. Phys. **91**, 7048 (1989).
[12] G. Chałasiński, M. M. Szczęśniak, S. M. Cybulski, and S. Scheiner, J. Chem. Phys. **91**, 7809 (1989).
[13] S. M. Cybulski, G. Chałasiński, and R. Moszyński, J. Chem. Phys. **92**, 4357 (1990); R. Moszyński, S. Rybak, S. Cybulski, and G. Chałasiński, Chem. Phys. Lett. **166**, 609 (1990).
[14] K. Watanabe and H. C. Anderson, J. Chem. Phys. **90**, 795 (1986).
[15] W. C. Swope and H. C. Anderson, J. Chem. Phys. **88**, 6548 (1984).
[16] D. D. Nelson, Jr., G. T. Fraser, K. I. Peterson, K. Zhao, W. Klemperer, F. J. Lovas, and R. D. Suenram, J. Chem. Phys. **85**, 5512 (1986).
[17] R. W. Bicks, Jr., G. Duquette, C. J. N. van den Meijdenberg, A. M. Rulis, G. Scoles, and K. M. Smith, J. Phys. B **8**, 3034 (1975).
[18] R. Brooks, F. Kalos, and A. E. Grosser, Mol. Phys. **27**, 1071 (1974).
[19] R. C. Cohen, K. L. Busarow, K. B. Laughlin, G. A. Blake, M. Havenith, Y. T. Lee, and R. J. Saykally, J. Chem. Phys. **89**, 4494 (1988).
[20] R. C. Cohen, K. L. Busarow, Y. T. Lee, and R. J. Saykally, J. Chem. Phys. **92**, 169 (1990).
[21] J. M. Hutson, J. Chem. Phys. **92**, 157 (1990).
[22] T. A. Dixon, C. H. Joyner, F. A. Baiocchi, and W. Klemperer, J. Chem. Phys. **74**, 6539 (1981).
[23] S. E. Novick, K. C. Janda, S. L. Holmgren, M. Waldman, and W. Klemperer, J. Chem. Phys. **65**, 1114 (1976).
[24] J. M. Steed, T. A. Dixon, and W. Klemperer, J. Chem. Phys. **70**, 4095 (1979).
[25] R. Viswanathan and T. R. Dyke, J. Chem. Phys. **82**, 1674 (1985).
[26] M. Losonczy, J. W. Moskowitz, and F. H. Stillinger, J. Chem. Phys. **59**, 3264 (1973).
[27] W. Kołos, G. Corongiu, and E. Clementi, Int. J. Quantum Chem. **17**, 775 (1980).
[28] R. Lascola and D. J. Nesbitt, private communication quoted in Ref. 21.
[29] F. J. Lovas, private communication quoted in Ref. 21.
[30] S. F. Boys and F. Bernardi, Mol. Phys. **19**, 553 (1970).
[31] M. Gutowski, F. B. van Duijneveldt, G. Chałasiński, and L. Piela, Mol. Phys. **61**, 233 (1987); Chem. Phys. Lett. **129**, 325 (1986).
[32] M. Gutowski, J. H. van Lenthe, J. Verbeek F. B. van Duijneveldt, and G. Chałasiński, Chem. Phys. Lett. **124**, 370 (1986).
[33] J. H. van Lenthe, J. G. C. M. van Duijneveldt–van de Rijdt, and F. B. van Duijneveldt, Adv. Chem. Phys. **69**, 521 (1987).
[34] G. Chałasiński and M. Gutowski, Chem. Rev. **88**, 943 (1988).
[35] P. Hobza and R. Zahradnik, Chem. Rev. **88**, 871 (1988); P. Hobza and R. Zahradnik, *Intermolecular Complexes. The Role of van der Waals Systems in Physical Chemistry and Biodisciplines* (Academia, Prague, 1988).
[36] (a) M. Gutowski, G. Chałasiński, and J. G. C. M. van Duijneveldt–van de Rijdt, Int. J. Quantum Chem. **26**, 971 (1984); (b) G. Chałasiński and M. Gutowski, Mol. Phys. **54**, 1173 (1985).
[37] B. Jeziorski and M. van Hemert, Mol. Phys. **31**, 713 (1976).
[38] (a) M. J. Frisch, J. S. Binkley, H. B. Schlegel, K. Raghavachari, C. F. Melius, R. L. Martin, J. J. P. Stewart, F. W. Bobrowicz, C. M. Rohlfing, L. R. Kahn, D. J. DeFrees, R. Seeger, R. A. Whiteside, D. J. Fox, E. M. Fluder, and J. A. Pople, GAUSSIAN 86, Carnegie-Mellon Quantum Chemistry Publishing Unit, Pittsburgh, PA, 1984; (b) S. M. Cybulski, TRURL package, 1989.
[39] A. Sadlej, Collect. Czech. Chem. Commun. **53**, 1995 (1988).
[40] G. Chałasiński, D. J. Funk, J. Simons, and W. H. Breckenridge, J. Chem. Phys. **87**, 3569 (1987).
[41] G. H. F. Diercksen and A. J. Sadlej, J. Chem. Phys. **96**, 17 (1985).
[42] Experimental parameters taken from G. H. F. Diercksen, B. O. Roos, and A. J. Sadlej, Int. J. Quantum Chem. **S17**, 265 (1983).
[43] C. Douketis, J. M. Hutson, B. J. Orr, and G. Scoles, Mol. Phys. **52**, 763 (1984).
[44] A. D. Buckingham and P. W. Fowler, J. Chem. Phys. **79**, 6426 (1983); Can. J. Chem. **63**, 2018 (1985).
[45] G. J. B. Hurst, P. W. Fowler, A. J. Stone, and A. D. Buckingham, Int. J. Quantum Chem. **29**, 1223 (1986).
[46] V. Magnasco, C. Costa, and G. Figari, Chem. Phys. Lett. **156**, 585 (1989).
[47] G. Chałasiński, J. H. Lenthe, and T. P. Groen, Chem. Phys. Lett. **110**, 369 (1984).
[48] G. Ravishanker, M. Mezei, and D. L. Beveridge, J. Chem. Soc. Faraday Trans. **17**, 55 (1982).
[49] L. R. Pratt and D. C. Chandler, J. Chem. Phys. **67**, 3683 (1977); **73**, 3430 (1980); **73**, 3434 (1980).
[50] A. Ben-Naim, J. Chem. Phys. **90**, 7412 (1990).
[51] P. Backx and S. Goldman, Chem. Phys. Lett. **113**, 578 (1985).
[52] Z. Latajka and S. Scheiner, J. Mol. Struct. **198**, 205 (1989).